Large-scale Linear Magnetic Holes with Magnetic Mirror Properties in Hybrid Simulations of Solar Wind Turbulence

Giuseppe Arrò[1] , Francesco Califano[2] , Francesco Pucci[3] , Tomas Karlsson[4] , and Hui Li[1]

[1] Los Alamos National Laboratory, Los Alamos, NM 87545, USA
[2] Dipartimento di Fisica "E. Fermi," Università di Pisa, Pisa, Italy
[3] Istituto per la Scienza e Tecnologia dei Plasmi, Consiglio Nazionale delle Ricerche, Bari, Italy
[4] Division of Space and Plasma Physics, School of Electric Engineering and Computer Science, KTH Royal Institute of Technology, Stockholm, Sweden
Received 2024 May 28; revised 2024 June 30; accepted 2024 July 10; published 2024 July 25

Abstract

Magnetic holes (MHs) are coherent magnetic field dips whose size ranges from fluid to kinetic scale, ubiquitously observed in the heliosphere and in planetary environments. Despite the long-standing effort in interpreting the abundance of observations, the origin and properties of MHs are still debated. In this Letter, we investigate the interplay between plasma turbulence and MHs, using a 2D hybrid simulation initialized with solar wind parameters. We show that fully developed turbulence exhibits localized elongated magnetic depressions, whose properties are consistent with linear MHs frequently encountered in space. The observed MHs develop self-consistently from the initial magnetic field perturbations by trapping hot ions with large pitch angles. Ion trapping produces an enhanced perpendicular temperature anisotropy that makes MHs stable for hundreds of ion gyroperiods, despite the surrounding turbulence. We introduce a new quantity, based on local magnetic field and ion temperature values, to measure the efficiency of ion trapping, with potential applications to the detection of MHs in satellite measurements. We complement this method by analyzing the ion velocity distribution functions inside MHs. Our diagnostics reveal the presence of trapped gyrotropic ion populations, whose velocity distribution is consistent with a loss cone, as expected for the motion of particles inside a magnetic mirror. Our results have potential implications for the theoretical and numerical modeling of MHs.

Unified Astronomy Thesaurus concepts: Solar wind (1534)

1. Introduction

Magnetic holes (MHs) are coherent magnetic field depressions observed ubiquitously in space. Satellite measurements have revealed the presence of MHs in the solar wind (SW; Turner et al. 1977; Winterhalter et al. 2000; Perrone et al. 2016; Yu et al. 2021), in planetary magnetosheaths (Volwerk et al. 2008; Génot et al. 2009; Madanian et al. 2020; Huang et al. 2021; Karlsson et al. 2021), in the Earth's magnetotail (Huang et al. 2019), and in cometary environments (Russell et al. 1987). The size of MHs is variable, ranging from hundreds of ion gyroradii ρ_i, to a few electron gyroradii ρ_e (Stevens & Kasper 2007). Henceforth, we will call "large-scale MHs" those MHs with size of about $10\,\rho_i$ or more. MHs are typically associated with local density and temperature enhancements, roughly balancing the magnetic pressure drop. The temperature increase is not isotropic, with higher temperatures perpendicular to the local magnetic field. The anticorrelation between the magnetic field and the density, together with the enhanced perpendicular temperature anisotropy, typically exceeding the mirror instability threshold, are all features hinting at a connection between MHs and mirror modes (Pantellini 1998). However, it is still unclear whether the mirror instability is actually capable of generating MHs. This problem has been investigated numerically by Califano et al. (2008) and Shoji et al. (2012) using hybrid simulations. Their studies have shown that the nonlinear stage of the mirror instability consists of a sequence of magnetic peaks and dips that merge over time,

producing mainly magnetic peaks, while holes develop only under very specific circumstances, rarely consistent with observations. Therefore, Califano et al. (2008) proposed that MHs may actually be a stable solution of the Vlasov–Maxwell system rather than a byproduct of the mirror instability. According to satellite measurements, mirror structures consisting of sequential peaks and dips and isolated magnetic peaks are generally observed in mirror-unstable environments (Soucek et al. 2008). Conversely, MHs are most often observed as isolated structures in mirror-stable regions (Balikhin et al. 2009). Hence, the occurrence of isolated MHs is hardly explained by models based on the mirror instability (Sundberg et al. 2015).

Turbulence has also been suggested as a possible driver for the formation of MHs, as the latter are often found in turbulent environments (Huang et al. 2017). This idea is corroborated by fully kinetic numerical simulations, showing that turbulent plasmas produce subion-scale MHs (Haynes et al. 2015; Roytershteyn et al. 2015; Arrò et al. 2023). The interplay between plasma turbulence and mirror instability has been investigated numerically by Hellinger et al. (2017), where a mirror-unstable plasma subject to turbulent perturbations has been considered. This work has shown that even in the presence of turbulence, a mirror-unstable plasma ultimately produces isolated magnetic peaks rather than MHs.

In this Letter, we investigate the formation and properties of large-scale MHs in a 2D hybrid simulation of plasma turbulence, starting from an initially mirror-stable plasma. We show an alternative mechanism for the generation of MHs, where strong magnetic fluctuations stabilize by trapping ions, eventually relaxing into long-lived MHs that coexist with fully developed turbulence. Despite the similarities with mirror
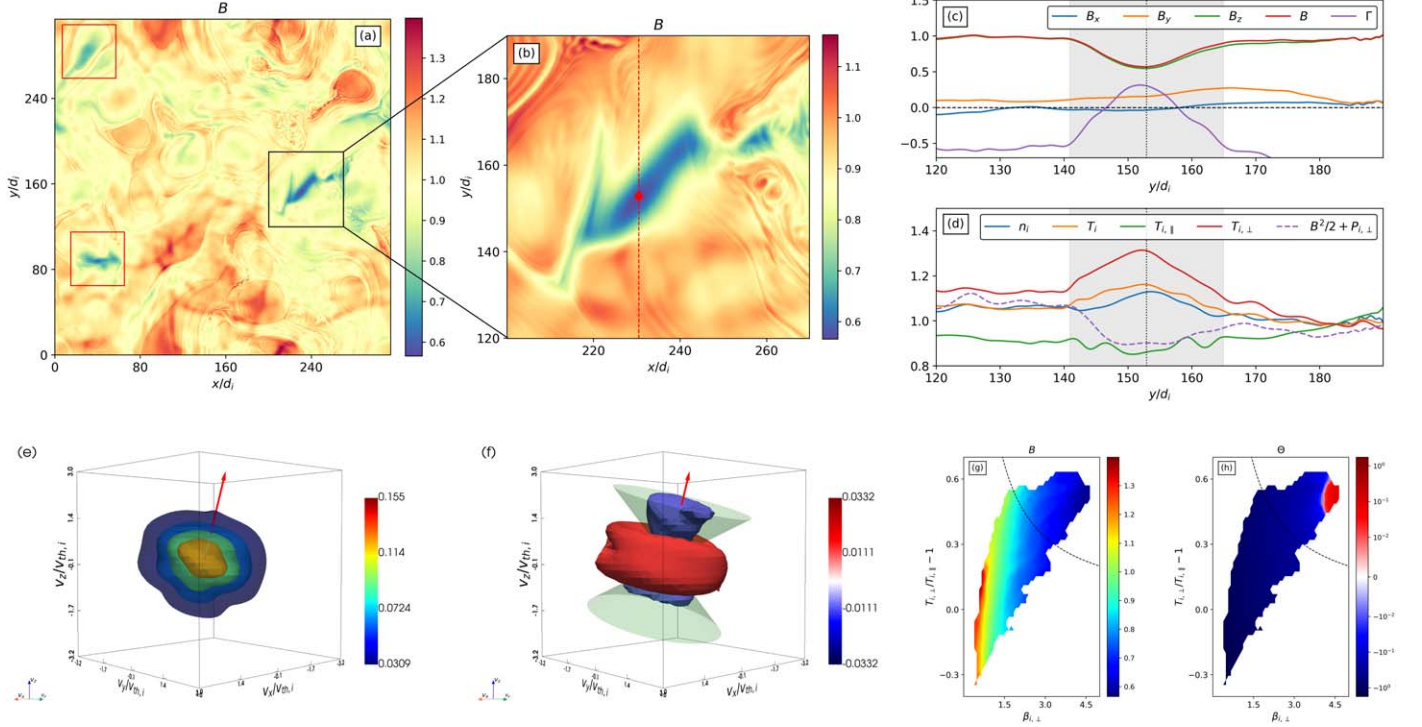
Figure 1. Magnetic field magnitude at $t = 543.5 \, \Omega_i^{-1}$ (a) with a zoom into an MH (b); magnetic field components and mirror threshold Γ (c), ion density, ion temperature components, and $B^2/2 + P_{i,\perp}$ (d) over the red dashed line in panel (b); 3D isosurfaces of f_i (e) and δf_i (f) at the red dot in panel (b) with local magnetic field (red arrow) and loss cone (green surface); magnetic field magnitude (g) and Θ (h) distributions in the $(T_{i,\perp}/T_{i,\parallel} - 1, \beta_{i,\perp})$ plane with the mirror threshold (black dashed line). The magnetic field, density, temperature, and $B^2/2 + P_{i,\perp}$ are in units of B_0, n_0, T_0, and $B_0^2/2 + n_0 T_0$, respectively.

modes, these stable MHs are not produced by the mirror instability, and their temperature anisotropy develops as a stabilizing effect rather than being the source of free energy for their formation.

2. Simulation Setup

Our simulation has been realized using the Eulerian hybrid Vlasov–Maxwell code (Valentini et al. 2007) with kinetic ions and fluid isothermal electrons with finite mass. The spatial domain is a 2D square periodic uniform grid with 3072^2 points and size $L = 100\pi \, d_i$, where d_i is the ion inertial length. The velocity domain is a 3D uniform grid with 51^3 points, with ion velocities v_x, v_y, v_z in the range $-5 \, v_{\mathrm{th},i} \leqslant v_x, v_y, v_z \leqslant +5 \, v_{\mathrm{th},i}$, where $v_{\mathrm{th},i}$ is the initial ion thermal speed. Ions are initially Maxwellian, with uniform density n_0, zero mean velocity, and isotropic temperature T_0 with unitary ion beta $\beta_i = 1$, implying $\rho_i \simeq d_i$. The ion-to-electron mass and temperature ratios are $m_i/m_e = 100$ and $T_i/T_e = 1$, respectively. The initial magnetic field includes a guide field $\boldsymbol{B_0} = B_0 \hat{\boldsymbol{z}}$, perturbed by random-phase, isotropic magnetic field fluctuations $\delta \boldsymbol{B}$, with wave-numbers k uniformly distributed in the range $1 \leqslant k/k_0 \leqslant 6$ (with $k_0 = 2\pi/L$) and root mean square (rms) amplitude $\delta B_{\mathrm{rms}}/B_0 \simeq 0.28$. These parameters aim at reproducing SW conditions (Bandyopadhyay et al. 2020). No external driving is employed, making the turbulence freely decaying. The simulation time step is $dt = 0.01 \, \Omega_i^{-1}$ (where Ω_i is the ion cyclotron frequency), and we stop the run at $t = 543.5 \, \Omega_i^{-1}$, when turbulence is fully developed. The final time is characterized by density fluctuations δn with rms amplitude $\delta n_{\mathrm{rms}}/n_0 \simeq 0.06$, magnetic field fluctuations with $\delta B_{\mathrm{rms}}/B_0 \simeq 0.18$, and velocity fluctuations $\delta \boldsymbol{u}$ with $\delta u_{\mathrm{rms}}/c_A \simeq 0.13$ (where $c_A = B_0/\sqrt{n_0}$ is the initial Alfvén speed; see Finelli et al. 2021

for additional information). We use a compact finite difference filter (Lele 1992) to smooth electromagnetic fluctuations at small scales, mimicking resistivity. The smoothing does not affect ion dissipation, the latter taking place at scales of a few d_i, because of kinetic effects (Arrò et al. 2020; Arró et al. 2022).

3. Results

In the first part of this section, we will examine the properties of MHs observed in our simulation at fully developed turbulence. We will then discuss the formation and evolution of MHs as turbulence develops.

Panel (a) of Figure 1 shows the magnetic field magnitude B over the whole simulation domain at fully developed turbulence ($t = 543.5 \, \Omega_i^{-1}$). A wide variety of structures at different scales are observed, including elongated regions where B suddenly drops. Panel (b) shows a zoom into one of these magnetic dips, whose length and width are about $30 \, d_i$ and $10 \, d_i$, respectively. This structure has properties consistent with large-scale MHs typically observed in space. Panels (c) and (d) show different quantities over a 1D cut crossing the MH, indicated by the red dashed line in panel (b). In panel (c), we see that the magnetic dip is mainly induced by the out-of-plane magnetic field B_z, which is dominant with respect to the in-plane components B_x and B_y. Additionally, neither B_x nor B_y show strong variations correlated with the hole, implying a weak magnetic field rotation across the MH. This property is typical of the so-called linear MHs (LMHs). The latter are usually observed in mirror-stable environments (Volwerk et al. 2021), which is also the case in our simulation. The mirror

instability threshold is (Southwood & Kivelson 1993)

$$\Gamma = \frac{T_{i,\perp}}{T_{i,\parallel}} - 1 - \frac{1}{\beta_{i,\perp}}, \qquad (1)$$

where $T_{i,\perp}$ and $T_{i,\parallel}$ are the perpendicular and parallel ion temperatures, respectively, with respect to the local magnetic field, and $\beta_{i,\perp}$ is the perpendicular ion beta. The threshold Γ is rigorously valid for bi-Maxwellian ions, but it is nonetheless a useful quantity to investigate the level of temperature anisotropy, largely used in observations. Panel (c) shows that the plasma exceeds the mirror threshold ($\Gamma > 0$) only inside the MH, while being mirror stable elsewhere. The ion density n_i and temperature T_i have a modest increase inside the MH, as observed in panel (d). The temperature variation is mainly induced by $T_{i,\perp}$, exhibiting a significant increase, while $T_{i,\parallel}$ slightly decreases. To understand the kinetic origin of density and temperature variations, we analyze the ion velocity distribution function (IVDF) f_i inside the MH. Panel (e) shows the 3D isosurfaces of f_i, at a position indicated by the red dot in panel (b) and by the vertical dotted line in panels (c) and (d). The IVDF is roughly gyrotropic, and ions have smaller velocities along the local magnetic field (red arrow), with a wider velocity spread in the perpendicular plane. The shape of f_i and the magnetic field configuration of the MH suggest that the structure may actually be able to selectively trap ions according to their velocity, similarly to magnetic mirrors. We thus investigate the IVDF evolution by comparing f_i with the initial Maxwellian distribution g_i. To this end, we calculate $\delta f_i = f_i - g_i$, with both f_i and g_i centered at the same mean velocity. A 3D representation of δf_i is shown in panel (f), together with the local loss cone (green surface), corresponding to

$$\left| \frac{v_\parallel}{v_\perp} \right| = \sqrt{\frac{B_{out}}{B_{in}} - 1} = \sqrt{\frac{B_0}{B} - 1} = \frac{1}{\tan(\theta_p)}, \qquad (2)$$

where $|v_\parallel/v_\perp|$ is the parallel-to-perpendicular particle velocity ratio. $B_{in} = B$ is the magnetic field inside the MH, while B_{out} is the magnetic field outside the structure, roughly equal to the guide field B_0, as seen in panel (c). Ions with a pitch angle larger than θ_p are confined by the magnetic field configuration, while other ions escape. We see that δf_i is positive outside the loss cone, meaning that the ion density in that portion of the velocity space has increased because of trapped ions. On the other hand, δf_i is negative inside the loss cone, implying that ions with small pitch angles have escaped the MH, reducing the density in the corresponding region of the velocity space. This analysis shows that the IVDF evolution is consistent with the dynamics of trapped and escaping ions, which also explains the observed temperature anisotropy inside the MH. In other words, the increase in $T_{i,\perp}$ and the slight decrease in $T_{i,\parallel}$ observed inside the MH are caused by the fact that ions with a large pitch angle are trapped by the structure, while other ions escape. The net effect of this dynamic is the development of a perpendicular temperature anisotropy above the mirror instability threshold.

Beside the MH we have analyzed so far, two more MHs with analogous properties are present in our simulation within the red boxes in panel (a) of Figure 1. To conveniently visualize the properties of all the MHs in the simulation, we analyze the distribution of B in the ($T_{i,\perp}/T_{i,\parallel} - 1$ versus $\beta_{i,\perp}$) plane. We

also introduce the trapping threshold Θ to determine if magnetic structures can trap ions. Θ is derived by taking the square of Equation (2), which gives

$$\Theta = \frac{B_0}{B} - 1 - \frac{T_{i,\parallel}}{T_{i,\perp}}, \qquad (3)$$

where we have used $(v_\parallel/v_\perp)^2 \sim T_{i,\parallel}/T_{i,\perp}$, giving the average parallel-to-perpendicular ion thermal velocity ratio. $\Theta > 0$ implies that ions are trapped by the local magnetic field on average. Panels (g) and (h) of Figure 1 show the distributions of B and Θ, respectively. The black dashed line represents the mirror instability threshold $T_{i,\perp}/T_{i,\parallel} - 1 = 1/\beta_{i,\perp}$. We see a monotonic tendency for regions with low B to lie above the mirror threshold. Furthermore, the deepest magnetic depressions efficiently trap ions as $\Theta > 0$. Hence, MHs in our simulation behave as magnetic mirrors, trapping ions and developing a perpendicular temperature anisotropy that exceeds the mirror threshold.

Our analysis at fully developed turbulence suggests that MHs are not produced by the mirror instability, since they are surrounded by a mirror-stable plasma, and their enhanced perpendicular temperature anisotropy develops as a consequence of ion trapping. We thus choose the MH of Figure 1 and follow its evolution over time to understand its generation process. Figure 2 shows B (first row), Γ (second row), and Θ (third row) around the developing MH at different time steps (corresponding to different columns). The first column shows that a mirror-stable ($\Gamma < 0$) magnetic depression is present since $t = 0\ \Omega_i^{-1}$, induced by initial fluctuations. Θ is positive inside the magnetic dip, meaning it can trap ions. The second column shows that this initial magnetic dip has evolved into an MH after $180\ \Omega_i^{-1}$. The magnetic structure has become thinner, with sharper boundaries, and the temperature anisotropy has grown above the mirror threshold ($\Gamma > 0$) as a consequence of ion trapping. Θ is also positive inside the MH, but it has become more localized and weaker in amplitude. After its development, the MH remains stable, and its properties are not significantly altered by the surrounding turbulence, whose main effect is to perturb the shape of the structure. By comparing the third and fourth columns of Figure 2, we see a tendency for the MH to stay tied to a bundle of magnetic field lines, indicated by the in-plane isolines. The turbulence shakes the magnetic bundle over time, and the MH adjusts its position and shape accordingly without noticeable variations in the values of B and Γ. We note that the MH is elongated across the magnetic bundle while being thinner along magnetic field lines. We argue that the width of the MH along magnetic field lines could be determined by the distance traveled by trapped ions, while the MH length across the magnetic bundle is roughly constant over time, likely determined by the size of the initial fluctuation. The same kind of temporal evolution and properties are observed also for the other MHs developing in the simulation.

As a final remark, we note that the MH remains quasi-stable despite its temperature anisotropy exceeding the mirror instability threshold. This is because the mirror threshold refers to a situation where linear perturbations develop over a homogeneous background, while the MH is a nonlinear structure, far from being homogeneous. Furthermore, the MH size is comparable to the typical wavelength of mirror modes, so local homogeneity is not a suitable assumption either, and
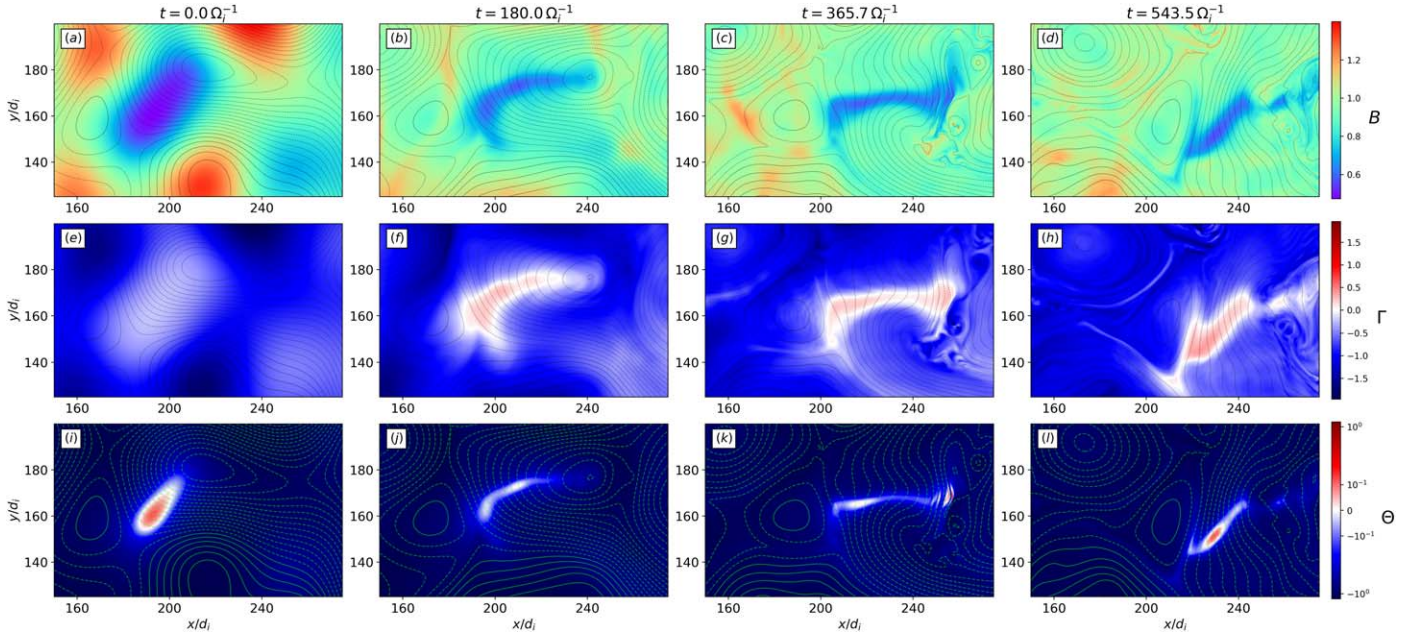
Figure 2. Magnetic field magnitude (in units of B_0; (a)–(d)), mirror threshold Γ ((e)–(h)), and Θ ((i)–(l)) at different times, showing the MH formation (with isolines indicating the in-plane magnetic field). Each column corresponds to a different time, given in the column title.

linear mirror theory does not apply. From a dynamical standpoint, temperature variations inside the MH produce a pressure force that helps sustaining the magnetic depression. Thus, the enhanced temperature anisotropy plays a stabilizing effect rather than being a source of free energy for instabilities, as confirmed by Figure 2, where the MH appears quasi-stable for hundreds of ion gyroperiods, with no unstable wave activity observed. In other words, when the MH is perturbed by the surrounding turbulence, its temperature anisotropy does not provide free energy for perturbations to grow, but instead, it helps making the structure more stable against turbulent fluctuations. This behavior is different with respect to that of other common structures produced by turbulence, such as current sheets, which become unstable once perturbed, breaking apart into magnetic islands and losing their identity as structures. As can be inferred from panels (c) and (d) of Figure 1, the MH is not exactly in pressure balance, likely because of turbulence, which explains why the structure is quasi-stable but not stationary. From a quantitative perspective, our analysis of the IVDF inside the MH shows that ions are almost gyrotropic, with perpendicular pressure $P_{i,\perp} = n_i T_{i,\perp}$. In this case, a perfect pressure balance would imply $\nabla_\perp (B^2/2 + P_{i,\perp}) \simeq 0$ across the MH (Zhang et al. 2017). Panel (d) of Figure 1 shows that $B^2/2 + P_{i,\perp}$ is roughly constant around the center of the MH outside the structure but not at its boundaries. Hence, the MH is not completely in pressure balance, and pressure gradients at its edges induce variations in its shape over time. We argue that the MHs we observe could be a metastable Vlasov equilibrium, as proposed in Califano et al. (2008), perturbed by the ambient turbulence. This aspect will be investigated in future studies.

4. Discussion and Conclusions

In this Letter, we have investigated the formation and properties of large-scale MHs using a 2D hybrid simulation of SW turbulence. We have shown that large-amplitude magnetic fluctuations can trap ions, similarly to magnetic mirrors, evolving into LMHs. Ions trapped inside MHs exhibit a velocity distribution consistent with a loss cone and induce a strong perpendicular temperature anisotropy above the mirror threshold, stabilizing the structure. The resulting MHs persist for hundreds of ion gyroperiods, being mildly affected by the surrounding mirror-stable turbulence. All these features, in particular the capability of MHs to trap ions, quantified by Θ, and the corresponding kinetic signatures in IVDFs, provide new criteria to define and identify MHs in satellite observations and numerical simulations. Our work shows that MHs in fully developed turbulence effectively represent a potential well that traps hot ions with large pitch angles. Thus, MHs potentially play a significant role in regulating the temperature anisotropy of turbulent plasmas such as the SW, given their abundance in these environments (Yu et al. 2021).

In this work, all the observed MHs develop from the initial magnetic field fluctuations used to drive turbulence. Initial fluctuations have an rms amplitude consistent with SW observation (Bandyopadhyay et al. 2020) but can be quite strong locally. It is reasonable to think that strong local fluctuations could be spontaneously produced by SW turbulence, where energy cascades from scales much larger than the MH size. Additionally, local magnetic reconnection events may also produce strong magnetic depressions (Pritchett & Mozer 2009). However, simulating the SW cascade from hundreds of d_i, retaining ion kinetic effects, is an extremely challenging problem. Hybrid particle-in-cell (PIC) codes can handle very large systems, but ion heating is sensitive to numerical noise (Franci et al. 2015). Since anisotropic ion heating is necessary to produce MHs, we employed a Eulerian Vlasov code, which is noise free but computationally much more expensive than PIC codes. Therefore, our approach is a trade-off between numerical accuracy and a sufficiently realistic representation of SW turbulence. Nonetheless, we have shown that strong local magnetic depressions relax to stable MHs rather than being assimilated and destroyed by turbulence. However, our study leaves open the question of understanding how large-amplitude magnetic fluctuations that

seed the formation of MHs may develop in a turbulent environment where energy is injected at scales much larger than the MH's size.

Understanding whether MHs in the heliosphere and planetary magnetosheaths originate in situ or come from neighboring environments is another open problem regarding these structures. One hypothesis is that MHs develop close to the Sun and are then advected by the turbulent SW. Karlsson et al. (2022) have shown that MHs of SW origin can cross planetary bow shocks and enter the magnetosheath, where conditions for local generation are hardly met. In this context, our results show that MHs are a stable element of turbulence, supporting the idea that they can be locally generated in the SW and then transported to planets and other regions in the heliosphere. Additional factors that have not been considered in this work, such as the SW expansion and 3D effects, may also influence the stability of MHs in SW turbulence and will be addressed in future studies.

ORCID iDs

Giuseppe Arrò ⓘ https://orcid.org/0000-0001-7233-2555
Francesco Califano ⓘ https://orcid.org/0000-0002-9626-4371
Francesco Pucci ⓘ https://orcid.org/0000-0002-5272-5404
Tomas Karlsson ⓘ https://orcid.org/0000-0002-4546-5050
Hui Li ⓘ https://orcid.org/0000-0003-3556-6568

References

Arrò, G., Califano, F., & Lapenta, G. 2020, A&A, 642, A45
Arró, G., Califano, F., & Lapenta, G. 2022, A&A, 668, A33
Arrò, G., Pucci, F., Califano, F., Innocenti, M. E., & Lapenta, G. 2023, ApJ, 958, 11
Balikhin, M., Sagdeev, R., Walker, S., et al. 2009, GeoRL, 36, L03105
Bandyopadhyay, R., Sorriso-Valvo, L., Chasapis, A., et al. 2020, PhRvL, 124, 225101
Califano, F., Hellinger, P., Kuznetsov, E., et al. 2008, JGRA, 113, A08219
Finelli, F., Perri, S., Sisti, M., & Califano, F. 2021, A&A, 656, A43
Franci, L., Landi, S., Matteini, L., Verdini, A., & Hellinger, P. 2015, ApJ, 812, 21
Génot, V., Budnik, E., Hellinger, P., et al. 2009, AnGeo, 27, 601
Haynes, C. T., Burgess, D., Camporeale, E., & Sundberg, T. 2015, PhPl, 22, 012309
Hellinger, P., Landi, S., Matteini, L., Verdini, A., & Franci, L. 2017, ApJ, 838, 158
Huang, S., He, L., Yuan, Z., et al. 2019, ApJ, 875, 113
Huang, S., Lin, R., Yuan, Z., et al. 2021, ApJ, 922, 107
Huang, S., Sahraoui, F., Yuan, Z., et al. 2017, ApJL, 836, L27
Karlsson, T., Heyner, D., Volwerk, M., et al. 2021, JGRA, 126, e2020JA028961
Karlsson, T., Trollvik, H., Raptis, S., Nilsson, H., & Madanian, H. 2022, AnGeo, 40, 687
Lele, S. K. 1992, JCoPh, 103, 16
Madanian, H., Halekas, J., Mazelle, C., et al. 2020, JGRA, 125, e2019JA027198
Pantellini, F. G. 1998, JGRA, 103, 4789
Perrone, D., Alexandrova, O., Mangeney, A., et al. 2016, ApJ, 826, 196
Pritchett, P., & Mozer, F. 2009, JGRA, 114, A11210
Roytershteyn, V., Karimabadi, H., & Roberts, A. 2015, RSPTA, 373, 20140151
Russell, C., Riedler, W., Schwingenschuh, K., & Yeroshenko, Y. 1987, GeoRL, 14, 644
Shoji, M., Omura, Y., & Lee, L.-C. 2012, JGRA, 117, A08208
Soucek, J., Lucek, E., & Dandouras, I. 2008, JGRA, 113, A04203
Southwood, D. J., & Kivelson, M. G. 1993, JGRA, 98, 9181
Stevens, M., & Kasper, J. 2007, JGRA, 112, A05109
Sundberg, T., Burgess, D., & Haynes, C. 2015, JGRA, 120, 2600
Turner, J., Burlaga, L., Ness, N., & Lemaire, J. 1977, JGR, 82, 1921
Valentini, F., Trávníček, P., Califano, F., Hellinger, P., & Mangeney, A. 2007, JCoPh, 225, 753
Volwerk, M., Mautner, D., Wedlund, C. S., et al. 2021, AnGeo, 39, 239
Volwerk, M., Zhang, T., Delva, M., et al. 2008, JGRE, 113, E00B16
Winterhalter, D., Smith, E. J., Neugebauer, M., Goldstein, B. E., & Tsurutani, B. T. 2000, GeoRL, 27, 1615
Yu, L., Huang, S., Yuan, Z., et al. 2021, ApJ, 908, 56
Zhang, X.-J., Artemyev, A., Angelopoulos, V., & Horne, R. 2017, JGRA, 122, 10